Nanometer-scale bioimaging via tunable terahertz plasmons

Hasan Tahir Abbas,[1,2] Xiaodong Zeng,[3, a)] Robert D. Nevels,[1] and M. Suhail Zubairy[3, b)]
[1)] *Department of Electrical and Computer Engineering, Texas A&M University, College Station, TX 77843 USA*
[2)] *Department of Electrical and Computer Engineering, Texas A&M University at Qatar, Doha, Qatar*
[3)] *Institute for Quantum Science and Engineering (IQSE) and Department of Physics and Astronomy, Texas A&M University, College Station, Texas 77843-4242, USA*

A nanometer-scale structured illumination microscopy (SIM) scheme via tunable plasmons is proposed. The sample is placed on a semiconductor heterostructure where terahertz plasmons generated by a current-driven instability, illuminate it. Full coverage of the spatial frequency regime is obtained by tuning the plasmons through the control on gate voltage. Hence, it is possible to reconstruct an image with a resolution up to two orders of magnitude beyond the diffraction limit. Due to the linear nature of the technique, only a weak illumination signal is required, therefore which minimizes the likelihood of sample damage and has potential applications in bioimaging.

In conventional wide-field fluorescence microscopy, the resolution of the system is half the wavelength of light due to the Abbe diffraction limit. With an ever growing need to image minuscule objects especially in life sciences, several superresolution microscopies have been realized. Structured illumination microscopy (SIM)[1–5] is a wide-field technique in which a fine illumination pattern such as a sinusoidal standing wave is used to generate *Moiré fringes* in the observed image[2,3]. The high spatial frequency content is mathematically reconstructed from a series of images acquired by shifting the pattern. Theoretically, unlimited resolution can be achieved using a non-linear version of SIM.[4]. However, the requirement of high-level illumination intensity subjects the sample to significant damage such as thermal effects. Afterwards, it has been found that resolution beyond the classical diffraction limit by a factor greater than 2 can be realized when an object is illuminated by surface plasmons[6,7], which have much smaller wavelengths.

Current-drive plasmon instabilities have mainly been studied in the context of ionized gases for a long time[8]. An analogous activity leads to generation of plasmons in solid-state devices that has many interesting applications in the far-infrared frequency region[9–19]. More importantly and interestingly, the spatial frequency response of the device can be tuned by varying the gate voltage[20,21]. In this paper, a nanometer-scale imaging technique is proposed where subwavelength plasmons, generated by a current in a transistor channel that can be tuned by controlling gate voltage, form the illumination pattern required for SIM. The configuration effectively creates a much larger observable spatial frequency region as compared to a far-infrared (terahertz) wave. Due to the linear nature of the scheme, resolution of up to two orders of magnitude beyond the diffraction limit can be obtained with a weak field intensity, which produces little damage to the sample and may play an important role in bioimaging. In comparison with the metal based SIM where the plasmonic wavelength is fixed by a determined structure[6], the period of the plasmonic pattern can be controlled by varying the gate voltage. Moreover, in contrast to previous scheme based on graphene[7], our scheme uses surface current to excite the plasmons, which does not require any wavevector matching mechanism such as gratings. Thus our scheme can be realized in experiment more easily.

A schematic diagram of the proposed system which is similar to a transistor, is shown in Fig 1 where a 2DEG acting as a transistor channel is formed at the interface of two semiconductor materials with slightly different band-gap energies. Plasmons are generated in the channel when the source and drain terminals are driven by a current source. Due to reflections from the conducting boundaries, the channel region creates a cavity where the plasmons form a standing wave. The structure is backed by a gate terminal that spans the length L of the channel and is spaced a distance d below the 2DEG. The gate capacitively couples with the 2DEG, so the velocity as well as the concentration of electrons in the channel can be controlled by varying the gate voltage. A barrier layer of thickness h separates the sample from the 2DEG.

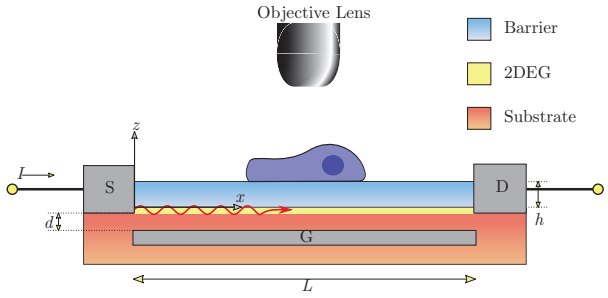

FIG. 1. (Color online) Illustration of the imaging scheme where the sample is excited by the standing plasmonic wave pattern generated in the 2DEG by a current-driven instability. Transistor arrangement with S, D, G denotes the source, drain and gate.

[a)] Electronic mail: zengxdgood@163.com
[b)] Electronic mail: zubairy@physics.tamu.edu

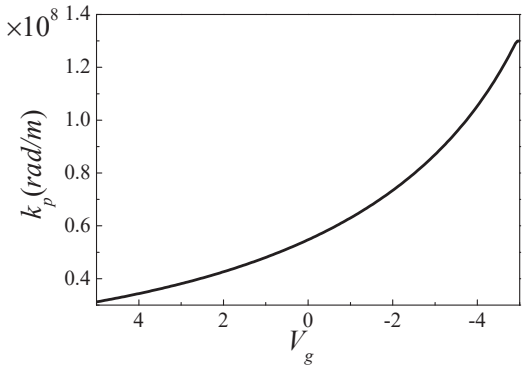

FIG. 2. Plasmon wave dispersion diagram for a transistor structure supporting a 2DEG channel. Here, $V_T = -9V$, $h = 20nm$ and $d = 120nm$.

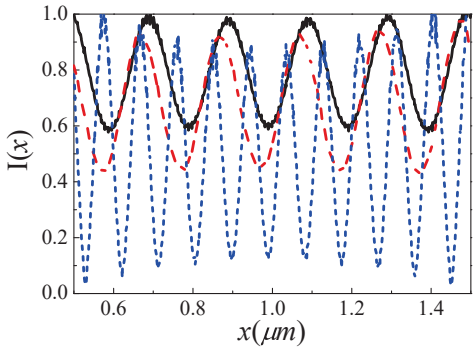

FIG. 3. Full-wave simulation results: Standing plasmonic wave patterns generated by a current-driven instability and an additional illumination at an angle χ. The field intensities are normalized. The surface current intensity is 1 mA/m and the incident wave amplitude is 0.5 V/m. The black solid and blue short dashed curves have incident angles $\chi = 0$ while the red dashed curve has an incident angle $\chi = 0.245$ rad. The corresponding gate voltages of the black solid, red dashed and blue short dashed curves are 5, 5 and $-0.4V$, respectively.

The compressed nature of the plasmons can be described by its dispersion relation. Here, we consider the sample stage which is terminated by a gate at the bottom and free-space at the top[22,23]. The 2DEG is modeled as a shunt admittance related to Drude-type surface conductivity[24], $\sigma_s = N_s e^2\tau/[m^*(1 - j\omega_p\tau)]$, where N_s is the surface electron density in the channel, e is the electron charge, m^* is the effective electron mass in the heterostructure, τ is the scattering time of electrons, and ω_p is the angular frequency. Through the gate voltage V_g, the electron density N_s of the channel can be varied as $N_s = N_0 \times (1 - V_g/V_T)$, where $N_0 = \varepsilon_2\varepsilon_0 V_T/ed$ is the zero-bias density, V_T is the gate threshold voltage of the transistor and ε_2 is the relative permittivity of the semiconductor substrate. The plasmonic dispersion relation can be written as $1 - r_u r_d e^{-2k_p h} = 0$. Here, r_u accounts for the reflection from the barrier to the vacuum while r_d refers to the reflection from the barrier to the substrate with 2DEG between them. Fig. 2 shows that the plasmonic wave number can be controlled by varying the gate voltage. The result is similar to the dispersion curve of gated 2DEG plasmons where the gate terminal is located above the barrier[25,26]. Here, the permittivity of both semiconductor layers is approximated to the static value, i.e., $\varepsilon_1 \approx \varepsilon_2 = 9.5$; the plasmon frequency is $10THz$; the mole-fraction of aluminum in AlGaN alloy is 0.1 and the scattering time τ is $1.14ps$ corresponding to a temperature of $77K$[27]. As the temperature is increased, τ gets smaller which leads to reduced mobility and induces larger loss in the channel. Compared with the vacuum wavenumber $2.09 \times 10^5 rad/m$, the figure demonstrates that the plamsonic wave vector can be hundreds of times larger than that in vacuum. A sample observed through such a high subwavelength illumination makes superresolution possible.

As discussed before, the 2DEG channel essentially behaves as a cavity due to the resonance effects introduced by the two conducting boundaries, i.e., drain and source terminals. Therefore, the plasmonic wavenumber k_p cannot be varied in a continuous fashion to cover all spatial frequencies. As an example, we set the length of the heterostructure and the resulting 2DEG channel to be $2\mu m$ in the simulation. Like any resonating structure, the plasmonic modes of the 2DEG channel are well-defined[27–29]. Fig. 3 shows simulations of plasmonic standing waves generated by a current-driven instability in the plasma channel (COMSOL). Here, the effective dielectric function of the 2DEG can be expressed as $\varepsilon(\omega_p) = \varepsilon_s - j\sigma_s/(\omega_p\Delta)$[30], where Δ is the 2DEG thickness and is set to be $2nm$ in our simulations. Due to the huge value of the plasmonic wave number, the electric fields along x direction and z direction of a plasmon near the 2DEG have almost the same amplitude but a phase difference $\pi/2$. Two counter-propagating plasmons along the 2DEG have a z component proportional to $e^{jk_p x}\mathbf{e}_z + e^{-jk_p x}\mathbf{e}_z = 2\cos(k_p x)\mathbf{e}_z$ and an x component proportional to $e^{jk_p x}\mathbf{e}_x - e^{-jk_p x}\mathbf{e}_x = 2\sin(k_p x)\mathbf{e}_x$. The total field intensity has a constant intensity[31]. Now we use a plane wave with an incident angle χ to illuminate the sample at the same time. The electric field of the plane wave can be expressed as $E_a(\cos\chi\mathbf{e}_x + \sin\chi\mathbf{e}_z)e^{jk_0\sin\chi x}$, where $E_a = E_0 e^{j\theta}$ is the amplitude. The total field intensity can be approximated as

$$\begin{aligned} &|2\cos(k_p x) + E_a\cos\chi e^{jk_0\sin\chi x}|^2 \\ &+ |2\sin(k_p x) + E_a\sin\chi e^{jk_0\sin\chi x}|^2 \\ &= 4 + |E_a|^2 + 4E_0\cos(\sin\chi k_0 x + \theta)\cos(k_p x - \chi). \end{aligned} \quad (1)$$

Due to $\sin\chi k_0 \ll k_p$, we can neglect the coefficient $\cos(\sin\chi k_0 x)$. The above expression describes a standing wave pattern with an effective period of $2\pi/k_p$. And, more remarkable, the phase shift can be controlled by the incident angle. The simulations in Fig. 3 also show that the standing wave patterns can be obtained and shifted by the surface current and an additional plane wave

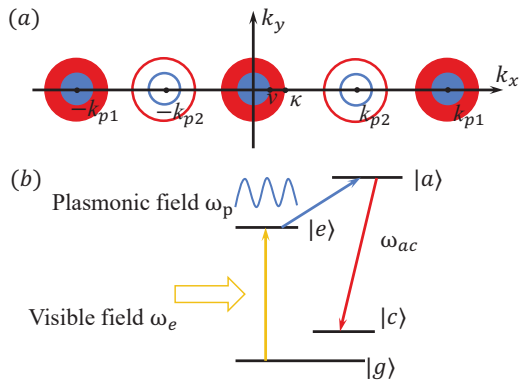

FIG. 4. (Color online) (a) Diagram of the spatial frequency distributions. The blue and red circles at the origin contribute to the conventional microscopy with imaging frequency ω_p and ω_{ac} respectively. The circles with the center at $\pm k_{p1/2}$ correspond to the linear response of the illumination pattern with period $2\pi/k_{p1/2}$. The period of the illuminating plasmons can be tuned by the gate voltage. (b) The energy structure of the sample molecule.

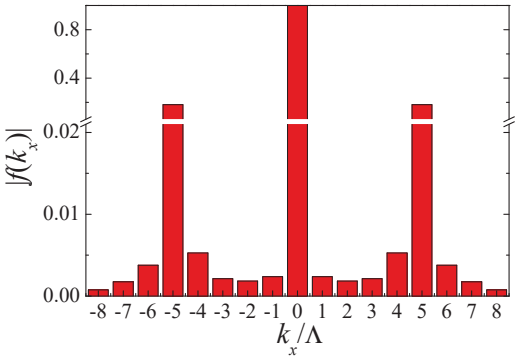

FIG. 5. The Fourier components of the red dashed line in Fig. 3. $\Lambda = 2\pi/S$ and $S = 1\mu m$ is the size of the sample along x.

incident from above.

In a linear SIM based on above surface plasmons, the illumination pattern $I(\boldsymbol{r})$ can be assumed sinusoidal and expressed as $I(\boldsymbol{r}) = C + (e^{j\boldsymbol{k}_p\cdot\boldsymbol{r}+j\phi} + e^{-j\boldsymbol{k}_p\cdot\boldsymbol{r}-j\phi})$, where C is a constant background, $\boldsymbol{k}_p$ is the plasmonic wavevector, and ϕ is the pattern phase. An image $M(\boldsymbol{r})$ of a sample molecule distribution $F(\boldsymbol{r})$ observed through a microscope can be expressed as

$$M(\boldsymbol{r}) \propto \int F(\boldsymbol{r}')I(\boldsymbol{r}') \cdot H(\boldsymbol{r}-\boldsymbol{r}')d\boldsymbol{r}', \qquad (2)$$

where $H(\boldsymbol{r})$ is the point spread function (PSF) of the microscope A spatial frequency domain representation of the image obtained by taking the Fourier transform is expressed as $\tilde{M}(\boldsymbol{k}) = \tilde{F}(\boldsymbol{k})\tilde{H}(\boldsymbol{k})$, where $\sim$ indicates a spatial frequency domain term, $\tilde{H}(\mathbf{k})$ is the optical transfer function (OTF) of the microscopy, and $\tilde{F}(\boldsymbol{k})$ is the Fourier transform of $F(\boldsymbol{r}) \cdot I(\boldsymbol{r})$. A spatial frequency representation of the scheme is illustrated in Fig. 4(a). In this scheme, we assume that the numerical aperture of the objective lens is unity. In conventional fluorescence microscopy, the observable spatial frequency is limited to a circle as shown in Fig. 4(a) where the passband is bounded by $(k_x^2 + k_y^2)^{1/2} = 2k_0 = 2\omega_p/c = \nu$. Since the plasmon frequency ω_p falls in the terahertz region, a relatively small k_0 implies that we need to image the sample a large number of times, which is time consuming. The process can be expedited by using an additional illumination field such as a laser with frequency ω_e. As shown in Fig. 4(b), the molecules in the sample are first excited from the ground level $|g\rangle$ to the excited level $|e\rangle$ by laser ω_e. The plasmonic wave then excites the molecules to an ancilla level $|a\rangle$. Utilizing the spontaneous decay of the molecules from $|a\rangle$ to $|c\rangle$, we image the sample with photons of frequency $\omega_{ac} = \omega_a - \omega_c$. A frequency-selective photonic crystal placed behind the objective lens can filter the photons of different frequencies[4]. As a consequence, the resulting passband in the spatial frequency domain is now bounded by $(k_x^2 + k_y^2)^{1/2} = 2k_{ac} = 2\omega_{ac}/c = \kappa$, which is the larger circle illustrated in Fig. 4(a). Since κ is much larger than ν, high resolution can be realized by imaging the sample only a few times.

A sinusoidal illumination pattern has three frequency components which, along with two shifted versions as shown in Fig. 4(a), generate an image from a linear combination of this frequency information. To reconstruct the sample, three different images need to be captured with each possessing a different phase term ϕ. The process can be expressed as a system of linear equations:

$$\tilde{F}(\boldsymbol{k}) = C\tilde{f}(\boldsymbol{k}) + \tilde{f}(\boldsymbol{k}-\boldsymbol{k}_p)e^{j\phi} + \tilde{f}(\boldsymbol{k}+\boldsymbol{k}_p)e^{-j\phi}. \qquad (3)$$

The phase shifts ϕ are known beforehand. Frequency content of the sample up to $k_p + \kappa$ can therefore be observed due to the *Moiré* effect which transports the high frequency information into the observation region. In order to obtain the three components of the spatial frequency as shown in above equation, we need to shift the plasmonic patterns. Our simulation results show that an additional incident plane wave can shift the pattern effectively. In Fig. 3, the red dashed curve shows the shift of the standing wave. Slight changes of the incident angles result in different phase variations which are needed to solve the spatial frequency in Eq. (3). To achieve two-dimensional enhancement in resolution, we can either rotate the sample or vary the angular distribution of the illumination.

Efficient production of plasmons with discrete wave numbers is accomplished due to the resonator effect in the transistor channel. The mode separation can be approximated as $\Delta_k = 2\pi \times 10^6 rad/m$. Thus, full coverage of all the spatial frequencies cannot be accomplished just by tuning the plasmonic wavelengths,. However, as discussed earlier, through the larger circle shown in Fig. 4(a), all the spatial frequencies up to the plasmonic wavenumber can be recovered. For

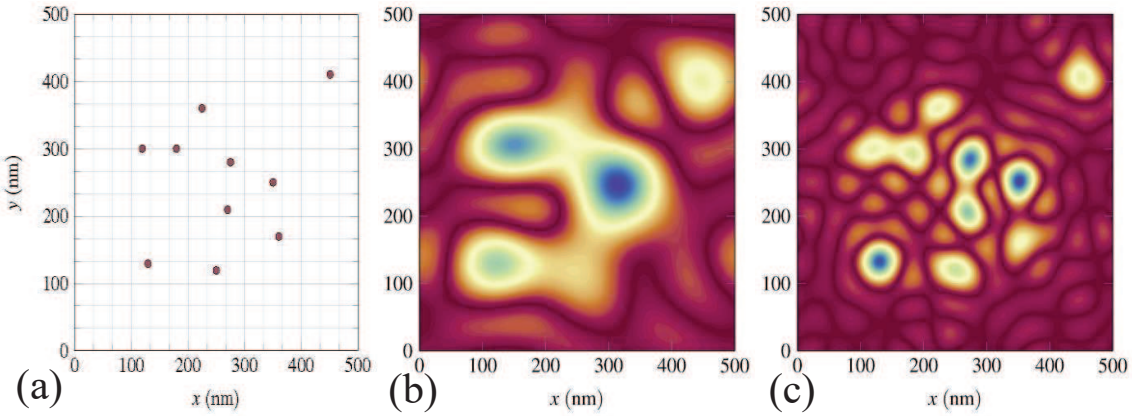

FIG. 6. (a) Sample distribution. Simulation of the reconstructed sample image at different parameters: (b) $Re(k_p^{max}) = 100k_0$ (c) $Re(k_p^{max}) = 300k_0$.

laser ω_e has a wavelength of 600nm, the circle radius is $\kappa = 4\pi/6 \times 10^7 rad/m$. Since $\Delta_k < \kappa$, all the spatial frequency can be obtained.

The boundaries and loss in the 2DEG affect the regularities of the field patterns. These irregularities mean that we cannot simply separate the spatial frequency into the three spatial frequency components as Eq. (3). However, if the sample size or even the transistor channel length is much smaller than the plasmons wave propagation length, i.e., $1/Im(k_p)$, the irregularities resulting from the loss can be neglected. With ever improving nanofabrication processing techniques, the loss along the 2DEG channel can be very small, which subsequently means a large $Re(k_p)/Im(k_p)$ ratio. Additionally, in order to improve the accuracy of the spatial frequency components, we do Fourier expansion on the field intensity, which is shown in Fig. 5. The figure shows that only a few larger Fourier components have values big enough to overcome the noise. As a consequence, equation (3) has several more terms and we still can obtain the spatial frequencies just by imaging the sample several more times. Due to the loss, the propagation distances of the plasmons are limited. In order to image a sample with large size, we can use laser ω_e to control the imaging area and in this area the field pattern is approximately periodical. After we image this area, we move the laser to another position and image the new area again. The whole sample can be imaged after scanning the sample by laser ω_e.

With all the Fourier information now known, an image of the sample can be reconstructed. We consider a sample with molecule distribution shown in Fig. 6(a). The minimum separation between the molecules is $38nm$ and maximum is $137nm$. The 2DEG plasmons have a frequency of 10THz and the numerical aperture (NA) is assumed to be 1. The reconstruction involves contributions from the spatial content up to a circular region of radius $k_p + \kappa$, where k_p can be manipulated by gate voltage. In Figs. 6(b) and 6(c), reconstructed images with maximum plasmonic wavenumber 100 and 300 times larger than the vacuum wavenumber are shown corresponding to 150nm and 75nm resolution, respectively. Fig. 6(b) shows that particles separated by a distance less than $75nm$ cannot be resolved and appear as a contiguous blurry streak, whereas they are distinguishable in Fig. 6(c). This demonstrates that our schema can technically obtain extremely high resolution.

Due to the large circle radius κ shown in Fig. 4(a), a total of only 30 to 50 images are required for the final image reconstruction, which in terms of imaging speed is very fast and is comparable to traditional nonlinear SIM[4]. However, unlike nonlinear SIM, the method described here requires only weak illumination intensity.

In this paper we have proposed a super-resolution microscopy scheme based on the subwavelength surface electromagnetic plasmons found in a semiconductor heterostructure. This method is useful in particular for light-sensitive samples as it requires weak field intensity for illumination, which can be used in bioimaging. Compared to metal based SIM where the plasmonic wavelengthes are fixed, the plasmonic pattern can be controlled by varying the gate voltage. Moreover, compared to the scheme based on graphene[7], our scheme uses surface current to excite the plasmons, no complex wavevector matching structure is needed and it can be easier realized in experiment.

ACKNOWLEDGMENTS

This research is supported by National Priorities Research Program (NPRP) Grant No. 8-352-1-074 from the Qatar National Research Fund (QNRF) .

[1] M. G. L. Gustafsson, J. Microsc. **198**, 82-87 (2000).
[2] R. Heintzmann and C. G. Cremer, Proc. SPIE. **3568**, 185-195 (1999).
[3] R. Heintzmann and G. Ficz, Brief Funct Genomic Proteomic. **5**, 289-301 (2006).
[4] M. G. L. Gustafsson, PNAS **102**, 13081-13086 (2005).

[5]X. Zeng, M. Al-Amri, Z. Liao, and M. S. Zubairy, Phys. Rev. A **91**, 063811 (2015).
[6]F. Wei and Z. Liu, Nano Lett. **10**, 2531-2536 (2010).
[7]X. Zeng, M. Al-Amri, and M. S. Zubairy, Phys. Rev. B **90**, 235418 (2014).
[8]A. B. Mikhailovskii, (Springer, 2013).
[9]K. Kempa, P. Bakshi, J. Cen, and H. Xie, Phys. Rev. B **43**, 9273 (1991).
[10]G. C. Dyer, X. Shi, B. V. Olson, S. D. Hawkins, J. F. Klem, E. A. Shaner, and W. Pan, Appl. Phys. Lett. **108**, 013106 (2016).
[11]J. Wu, A. S. Mayorov, C. D. Wood, D. Mistry, L. Li, W. Muchenje, M. C. Rosamond, L. Chen, E. H. Linfield, A. G. Davies, and J. E. Cunningham, Sci. Rep. **5**, 15420 (2015).
[12]F. Stern, Phys. Rev. Lett. **18**, 546 (1967).
[13]S. J. Allen, Jr., D. C. Tsui, and R. A. Logan, Phys. Rev. Lett. **38**, 980 (1977).
[14]M. Dyakonov and M. Shur, Phys. Rev. Lett. **71**, 2465 (1993).
[15]M. Dyakonov and M. Shur, IEEE Trans. Electron Devices **43**, 380-387 (1996).
[16]V. V. Popov, G. M. Tsymbalov, M. S. Shur, and W. Knap, Semiconductors **39**, 142-146 (2005).
[17]T. Otsuji, M. Hanabe, T. Nishimura, and E. Sano, Opt. Express **14**, 4815-4825 (2006).
[18]M. Dyakonov and M. S. Shur, Appl. Phys. Lett. **87**, 111501 (2005).
[19]D. Hofstetter, L. Diehl, J. Faist, W. J. Schaff, J. Hwang, L. F. Eastman, and C. Zellweger, Appl. Phys. Lett. **80**, 2991 (2002).
[20]A. E. Fatimy, N. Dyakonova, Y. Meziani, T. Otsuji, W. Knap, S. Vandenbrouk, K. Madjour, D. Théron, C. Gaquiere, M. A. Poisson, S. Delage, P. Prystawko, and C. Skierbiszewski, J. Appl. Phys. **107**, 024504 (2010).
[21]S. Rabbaa and J. Stiens, J. Phys. D: Appl. Phys. **44**, 325103 (2011).
[22]R. Kastner, E. Heyman, and A. Sabban, IEEE Trans. Antennas Propag. **36**, 1204-1212 (1988).
[23]K. A. Michalski, Encyclopedia of RF and Microwave Engineering, (John Wiley & Sons, Inc., 2005).
[24]P. J. Burke, I. B. Spielman, J. P. Eisenstein, L. N. Pfeiffer, and K. W. West, Appl. Phys. Lett. **76**, 745 (2000).
[25]M. Nakayama, J. Phys. Soc. Jpn. **36**, 393-398 (1974).
[26]A. Eguiluz, T. K. Lee, J. J. Quinn, and K. W. Chiu, Phys. Rev. B **11**, 4989 (1975).
[27]A. V. Muravjov, D. B. Veksler, V. V. Popov, O. V. Polischuk, N. Pala, X. Hu, R. Gaska, H. Saxena, R. E. Peale, and M. S. Shur, Appl. Phys. Lett. **96**, 042105 (2010).
[28]V. V. Popov, A. N. Koudymov, M. Shur, and O. V. Polischuk, J. Appl. Phys. **104**, 024508 (2008).
[29]V. V. Popov, M. S. Shur, G. M. Tsymbalov, and D. V. Fateev,Int. J. High Speed Electron. Syst. **17**, 557-566 (2007).
[30]T. Ando, A. B. Fowler, and F. Stern, Rev. Mod. Phys. **54**, 437 (1982).
[31]X. Zeng, L. Fan, and M. S. Zubairy, Phys. Rev. A **95**, 053850 (2017).